Nanoscale

REVIEW

View Article Online
View Journal

Cite this: DOI: 10.1039/d5nr04002g

Interfacial mechanisms in the freezing of polymer solutions

Nicolas Gustav Ulrich and Jean-François Louf *

Freezing of polymer solutions plays a central role in processes such as cryopreservation, porous material synthesis, and environmental remediation. Unlike simple solutes, polymers influence solidification through chain exclusion, interfacial adsorption, and confinement effects. These interactions shape the structure and stability of the freezing front and lead to solute gradients, phase separation, or morphological instabilities. In this review, we examine the physical mechanisms that govern polymer redistribution during freezing. We describe how polymer properties affect front morphology, survey experimental approaches for tracking solute dynamics, and discuss modeling strategies that link molecular behavior to macroscopic structure. We highlight recent advances in cryo-imaging and simulation, and identify open questions at the intersection of transport, thermodynamics, and interfacial physics.

Received 23rd September 2025,
Accepted 7th January 2026

DOI: 10.1039/d5nr04002g

rsc.li/nanoscale

1. Introduction

Freezing of polymer solutions plays a central role in systems ranging from cryopreservation and food processing to the fabrication of porous scaffolds through ice templating.[1–8] In these systems, the presence of long-chain molecules introduces behaviors that differ markedly from those in simple aqueous solutions.[9] As ice grows, polymer chains are typically excluded from the solid phase due to unfavorable enthalpic and entropic interactions.[10] This rejection leads to solute enrichment near the freezing front, alters local transport properties, and modifies the stability and shape of the advancing interface.[11,12] A useful point of comparison is the freezing of salt solutions, where similar solute rejection and interfacial instabilities arise from constitutional undercooling. However, polymer solutions differ in several key respects: polymer diffusivities are orders of magnitude lower than ionic diffusivities, transport is often nonlinear due to concentration-dependent viscosity and crowding, and polymers may adsorb to the ice interface or bind water, altering interfacial kinetics in ways not typically captured by purely colligative models.[13–15] Recent work on salty droplets and seawater freezing highlights how ionic redistribution remains largely diffusion-controlled at the nanoscale,[14,15] whereas polymer systems frequently enter regimes dominated by rheological arrest, kinetic trapping, or vitrification, producing qualitatively different front dynamics and frozen microstructures.

The interplay between polymer exclusion,[16] adsorption,[17] and local confinement[12] generates complex interfacial dynamics.[18] Concentration gradients that arise near the front impact thermal and mechanical properties of the unfrozen phase,[9,19] potentially leading to microphase separation,[20–23] viscosity changes,[24] or vitrification.[25,26] In some systems, partial adsorption of polymers onto ice modifies surface energy and step kinetics, further influencing the evolution of the front.[27] These processes act simultaneously, creating feedback loops that shape both the microstructure of the solidified material and the conditions under which freezing proceeds.[28]

Morphological outcomes depend sensitively on polymer characteristics such as chain length, flexibility, and concentration, as well as on external parameters like freezing rate,

Chemical Engineering Department, Auburn University, USA.
E-mail: jlouf@auburn.edu

Jean-François Louf

Jean-François Louf is an Assistant Professor of Chemical Engineering at Auburn University. His research investigates how coupled fluid, elastic, and transport processes govern behavior in living and soft materials. Drawing on concepts from poroelasticity, polymer physics, fluid mechanics, and interfacial science, he combines experiments, theory, and advanced imaging to study how plants and soft matter systems respond to mechanical, acoustic, and thermal stimuli. His work bridges fundamental physics and materials design, with applications ranging from cryogels and porous materials to bio-inspired sensing, transport control, and energy-efficient technologies.

confinement geometry, and thermal gradient.[28,29] The resulting structures—lamellae, pores, dendrites, or vitrified domains—reflect the coupling between interfacial kinetics and bulk transport.[16,30] These patterns are not merely aesthetic outcomes but control properties such as mechanical strength, permeability, and porosity, making them critical in applications from tissue engineering to water purification.[31]

Recent advances in imaging and simulation have provided new insight into these coupled mechanisms. Cryogenic confocal microscopy, vibrational spectroscopy, and tomography now allow spatially resolved mapping of solute distributions and front morphology.[32–37] At the molecular scale, simulations reveal how polymer–ice interactions depend on chain chemistry and interfacial topology, offering a mechanistic view of adsorption, pinning, and exclusion dynamics.[38,39] These tools have also underscored the role of slow diffusion and nonlinear rheology in governing front behavior, particularly at high polymer concentrations.[3,11,12]

This review examines the fundamental physical mechanisms that govern freezing in polymer solutions, with a focus on interfacial interactions, solute transport, and front morphology. By drawing from recent experiments, simulations, and theoretical models, we aim to clarify how polymer properties and freezing conditions jointly determine solidification pathways. We identify common features across systems and highlight open questions that remain in connecting microscale phenomena to macroscopic outcomes.

2. Polymer–ice interactions at the interface

As ice forms in a polymer solution, the advancing solid–liquid interface encounters a medium with distinct physical properties: long-chain molecules, entropic elasticity, and solute-driven thermodynamic gradients.[19,40] Unlike low-molecular-weight solutes, polymers are generally excluded from the ice phase, resulting in a concentration boundary layer that can influence both the morphology and velocity of the growing front.[41] The dynamics in this interfacial region play a critical role in determining the structure of the frozen material.

2.1. Polymer exclusion and interfacial accumulation

As the ice front advances into a polymer solution, dissolved chains are typically rejected from the growing crystal lattice due to their large size, low diffusivity, and unfavorable enthalpic interactions.[42] This exclusion leads to the formation of a polymer-rich boundary layer ahead of the front.[43–45] The thickness and shape of this zone result from a competition between the motion of the front and the ability of solutes to diffuse away.[12] The balance between these effects is captured by the Peclet number (Pe),[46] which governs the structure of the accumulation layer and the severity of concentration gradients:

$$\mathrm{Pe} = \frac{VL}{D} \quad (1)$$

where V is the velocity of the freezing front, L is the characteristic thickness of the exclusion layer, and D is the polymer diffusivity. For Pe ≪ 1, diffusion dominates and solutes redistribute over broad distances. When Pe ≫ 1, the front outruns diffusion, leading to sharp, compressed concentration gradients (see Fig. 1a). This concentration buildup not only modifies transport but also governs the local rheological state.

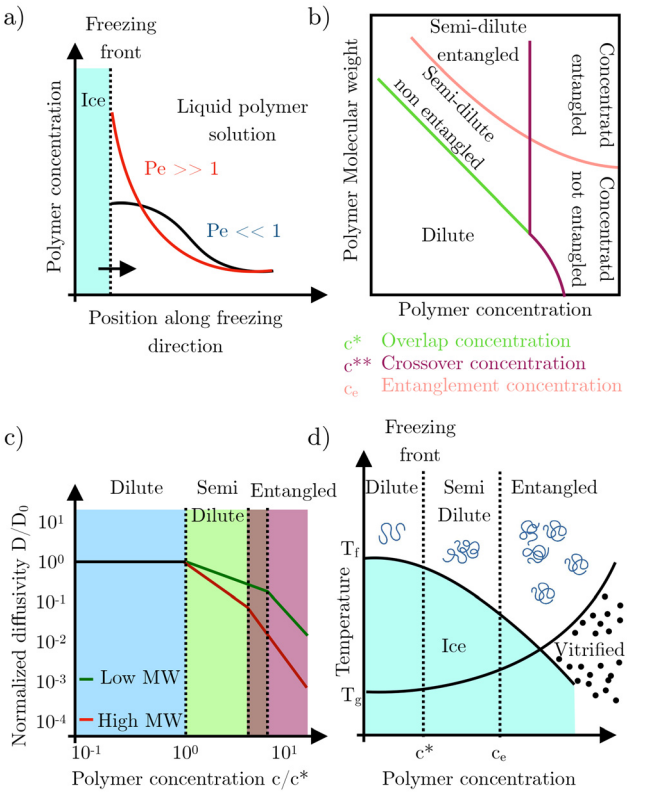

Fig. 1 (a) Schematic of polymer redistribution ahead of the freezing front, highlighting Peclet number regimes and accumulation gradients. (b) Concentration–molecular weight phase diagram adapted from Graessley[48] with permission from Elsevier, copyright 1980, showing how accumulation drives transitions between dilute, semi-dilute, and entangled states. Together, these panels link spatial solute dynamics to rheological and structural regimes relevant for front evolutions. (c) Schematic of the concentration-dependent polymer diffusion coefficient $D(c)$ for low and high molecular weight (MW) polymers. In the dilute regime ($c/c^* < 1$), both curves collapse to $D/D_0 = 1$ when normalized by the infinite-dilution diffusivity D_0. Above the overlap concentration ($c/c^* = 1$, first vertical dashed line), diffusivity decreases due to coil overlap and crowding, with high-MW polymers showing a steeper drop. Entanglement concentrations (c_e, second and third vertical dashed lines) occur at lower c/c^* for high-MW polymers, producing an earlier transition to the entangled regime and stronger suppression of diffusion. (d) Schematic phase diagram illustrating the dynamic states of a polymer solution as a function of temperature and concentration. Vertical lines indicate the overlap concentration c^* and the entanglement concentration c_e separating dilute, semi-dilute, and entangled regimes. The upward-curved boundary marks the condition $T = T_g(c)$, above which the solution remains fluid and below which vitrification occurs. As freezing proceeds and solutes accumulate ahead of the front, the local trajectory can traverse these boundaries, transitioning from a dilute to a vitrified state. This progression governs diffusion, viscoelasticity, and front morphology during solidification.

Depending on the molecular weight and freezing trajectory, the system may evolve from a dilute to an entangled or vitrified regime (Fig. 1b), with sharp consequences for mobility, front morphology, and thermodynamic behavior.[19,47]

In polymer solutions, however, D is not constant. As polymer chains accumulate, local viscosity increases and diffusion slows, creating a feedback loop that amplifies crowding near the front.[33] This effect can be captured by a scaling law of the form:

$$D(c) = D_0\left(\frac{c^*}{c}\right)^{\alpha} \quad (2)$$

where D_0 is the diffusivity at infinite dilution, c^* is the overlap concentration, and α ranges from 1 to 2 depending on polymer chemistry.[49–51] As the local concentration c approaches or exceeds c^*, diffusion becomes increasingly hindered, and the effective Peclet number rises dynamically during freezing,[52] a shown in Fig. 1c.

This concentration buildup not only alters transport but also affects thermodynamic and mechanical properties.[53] High local polymer content depresses the freezing point,[54] increases osmotic pressure, and may even lead to vitrification when the solution transitions into a glassy or phase-separated state.[24,55] If the front advances slowly enough, the boundary layer may reach the entanglement threshold c_e, where chains form a transient elastic network that resists deformation and further slows redistribution[18,32,56] (Fig. 1d).

Thus, polymer exclusion during freezing is governed by coupled gradients in concentration, viscosity, and diffusivity. Even small differences in polymer chemistry or freezing rate can lead to markedly different front behaviors—ranging from smooth stratification to unstable, highly heterogeneous solidification. These interfacial accumulation dynamics lay the foundation for morphological transitions discussed in later sections.

2.2. Interfacial adsorption and pinning

Beyond simple exclusion, many polymers exhibit transient or partial adsorption to the ice interface.[57,58] These interactions are often mediated by hydrogen bonding,[59] dipolar forces,[60] or surface hydration structure.[61] Even weakly adsorbing polymers can create energetic barriers to ice propagation by locally perturbing interfacial energy and inhibiting molecular alignment during crystallization.[62,63]

Molecular dynamics simulations have shown that poly(vinyl alcohol) (PVA) exhibits selective adsorption on prismatic ice faces, with adsorption events stabilized by hydroxyl groups aligning with the ice lattice.[64] However, this adsorption is not continuous: surface coverage proceeds slowly due to kinetic limitations, leading to heterogeneous distributions of bound chains along the front.[65] These patchy domains act as pinning sites that alter step flow and roughen the interface on the nanoscale.[58]

The physical picture of adsorption can be framed through a Langmuir-like model, where surface coverage θ increases with polymer concentration c as $\theta = K_c/(1 + K_c)$, with K a binding constant.[49] However, in freezing systems, the dynamics of adsorption propagation and the spatial arrangement of binding sites play a more critical role than equilibrium saturation.[66,67] Simulations and surface force measurements suggest that adsorbed chains can span multiple surface sites, creating multivalent anchoring points that resist front advance.[68,69]

Comparisons with antifreeze proteins (AFPs) provide a useful limiting case. AFPs exhibit irreversible adsorption and strong pinning,[58,70] completely arresting ice growth by binding to specific lattice motifs.[66,67,71] In contrast, polymers like PVA or PEG display reversible, mobility-limited interactions that allow partial rearrangement but still induce localized undercooling.[72] Atomic force microscopy (AFM) studies have confirmed these distinctions: AFPs form ordered, immobile layers, while polymers form disordered, loosely adsorbed clusters with finite residence times.[73] These contrasting behaviors are illustrated in Fig. 2 which shows simulation snapshots of PVA adsorption and AFP binding on ice, highlighting the spectrum of interfacial interactions that govern front morphology.

Adsorption also modifies interfacial energetics. Local changes in surface energy γ_{sl} affect the curvature and freezing point through the Gibbs–Thomson relation,[75,76] and the presence of protruding chains or bound layers can stabilize convex asperities or pin terrace edges. These microstructural effects shift the front morphology from faceted to cellular under directional freezing,[77] especially at low polymer concentrations where adsorption dominates over bulk accumulation.[78–80]

Altogether, interfacial adsorption provides a second mechanism, distinct from solute exclusion, through which polymers influence ice front dynamics.[81] Its impact is strongest at early stages of freezing or in low-concentration regimes, where even partial coverage can seed morphological transitions and guide solidification pathways.

2.3. The role of chain flexibility and confinement

The behavior of polymers near a freezing front is strongly influenced by their chain flexibility and the degree of confinement within the local exclusion layer.[65,68,82] These factors govern how polymers accumulate, orient, and redistribute during solidification, shaping the concentration gradients and interfacial dynamics that set the stage for subsequent morphological evolution.[83,84]

Flexible polymers, such as poly(ethylene glycol) (PEG) or poly(vinyl alcohol) (PVA), exhibit low persistence lengths and typically adopt coiled configurations in dilute solution.[85,86] As freezing progresses, excluded polymers accumulate ahead of the ice front, where the narrowing boundary layer compresses their conformational space.[19] This compression imposes entropic penalties that manifest as repulsive forces resisting further densification. The confinement free energy can be estimated as $F_{conf} \sim k_B T(R_g/R)^2$, where R_g is the polymer's radius of gyration and R is the effective thickness of the exclusion layer.[49,87,88] The result is a zone of heightened osmotic pressure and steric resistance near the interface.[89,90]

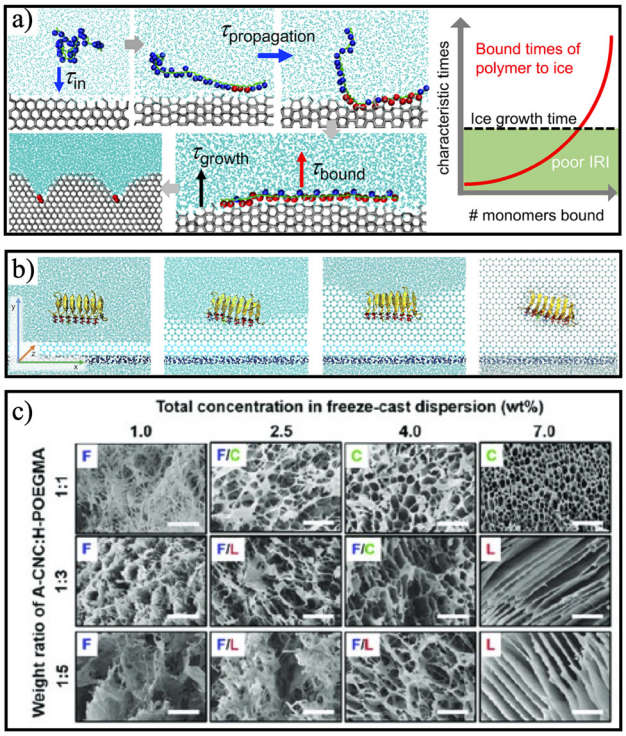

Fig. 2 Contrasting modes of macromolecular adsorption at the ice interface. (a) Molecular dynamics simulation showing partial, kinetically limited adsorption of poly(vinyl alcohol) (PVA) on the prismatic ice face. Despite strong binding affinity *via* hydroxyl groups, surface coverage proceeds slowly, resulting in heterogeneous roughness and localized growth inhibition. Figure adapted from Naullage and Molinero[65] with permission from the American Chemical Society, copyright 2020. (b) Simulation snapshot depicting insect antifreeze proteins (AFPs) irreversibly bound to specific ice lattice sites. The bound AFPs arrest step flow and facet propagation, inducing curvature and undercooling consistent with the Gibbs–Thomson equation. Together, these examples illustrate the spectrum of ice–macromolecule interactions: from dynamic, reversible adsorption in synthetic polymers to strong, lattice-specific pinning by biological antifreeze proteins; each modulating front morphology *via* distinct physical mechanisms. Figure reproduced from Gerhauser *et al.*,[71] with permission from the American Chemical Society, copyright 2021. (c) Cryo-SEM image of a collagen-based scaffold produced by directional freeze casting. The aligned lamellar structure reflects front destabilization and polymer retention during freezing. Adapted from Shahbazi *et al.*[74] Scale bars are 20 μm.

As local concentrations exceed the overlap threshold c^*, chains begin to interpenetrate, forming an entangled network with dramatically increased viscosity.[91,92] Above the entanglement concentration c_e, long-range chain constraints slow diffusion and trap heterogeneities. These viscoelastic changes feed back into solute redistribution and interface mobility, reinforcing gradients and potentially inducing local instabilities.

The persistence length l_p of the polymer chain further modulates these interactions.[93] Semi-rigid polymers, including chitosan and cellulose derivatives, interact anisotropically with the interface, often resisting compression and adopting stretched or aligned configurations.[37] AFM and cryo-imaging studies suggest that stiffer chains can form ordered domains or bridging contacts across rough ice features, locally modifying surface energy and promoting interfacial pinning.[73,94,95] Unlike flexible coils that deform to minimize entropic cost, stiff chains constrain the geometry of the exclusion layer, amplifying curvature effects and altering local undercooling patterns.[58]

Flexibility also affects kinetic trapping.[96] Polymers with short relaxation times can more readily rearrange and are thus more efficiently excluded, while stiffer or already-entangled chains may be partially trapped due to their limited configurational response times.[97,98] This leads to spatial variations in composition within the frozen phase, with enrichment or depletion zones determined by the interplay between chain mobility and front velocity.[99]

In summary, chain flexibility and local-scale confinement modulate the structure, dynamics, and rheology of the exclusion layer at the ice–solution interface. By influencing chain conformation, orientation, and relaxation behavior, these parameters control the initial conditions for larger-scale front morphology and the pore architecture formed during freezing.

2.4. Thermodynamic implications

The polymer-enriched boundary layer modifies local freezing conditions through both colligative and curvature-driven effects. As solutes accumulate near the front, the local freezing point is depressed due to both osmotic pressure and interface curvature.[12,100] For dilute solutions, the freezing point depression can be approximated by a Flory–Huggins-style expression:[101,102]

$$\Delta T_f = \frac{RT_f^2}{\Delta H_f}\left(\frac{\Phi}{M_n}\right) \quad (3)$$

where ΔT_f is the freezing point depression, R is the gas constant, T_f is the freezing point of the pure solvent, ΔH_f is the enthalpy of fusion, Φ is the polymer volume fraction, and M_n is the number-average molecular weight. This expression captures the dependence of colligative effects on polymer loading and chain size.

In addition to concentration-driven freezing point depression, the geometry of the freezing interface contributes through curvature effects. As the ice front becomes roughened or cellular, the local radius of curvature decreases, amplifying freezing point suppression through the Gibbs–Thomson effect:[103,104]

$$\Delta T_f = \frac{2\gamma_{sl}T_m}{\rho_s L_f r} \quad (4)$$

where γ_{sl} is the solid–liquid interfacial energy, T_m is the bulk melting point, ρ_s is the solid-phase density, L_f is the latent heat of fusion, and r is the radius of curvature.[71]

Adsorbed polymers influence interfacial energetics primarily by modifying local surface tension and stabilizing surface roughness, rather than by directly altering curvature.[62] These changes affect the distribution of undercooling along the front and can shift the energetic balance that governs step nuclea-

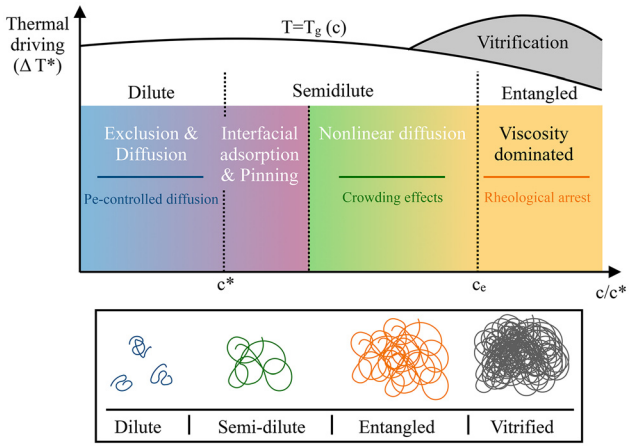

Fig. 3 Regime map for freezing of polymer solutions. Dominant freezing mechanisms are organized as a function of reduced polymer concentration c/c^* and thermal driving $\Delta T^* = T_f - T$. Vertical bands mark dilute, semi-dilute, and entangled solution regimes, while shaded regions indicate dominant interfacial or transport mechanisms, including diffusion-controlled exclusion, nonlinear diffusion and crowding, viscous arrest, interfacial adsorption, and vitrification upon crossing the concentration-dependent glass transition $T_g(c)$. Boundaries are schematic and denote crossover behavior.

tion or facet propagation. Regions of lower curvature or reduced polymer accumulation freeze preferentially, leading to spatial variations in front velocity and promoting morphological instabilities[12] under directional solidification.

Together, these effects—colligative depression and curvature amplification—act synergistically to determine where and how freezing initiates and propagates in polymer-rich environments. Markedly, the relative importance of these thermodynamic contributions depends on both the initial polymer concentration and the imposed thermal driving, which also control the transport and rheological state of the polymer-enriched boundary layer.

Fig. 3 synthesizes these coupled interfacial, transport, and thermodynamic mechanisms into an integrative nanoscale regime map, situating the local processes discussed above within the broader parameter space defined by polymer concentration and thermal driving.

3. Solute accumulation and redistribution

As the ice front advances through a polymer solution, solutes are typically excluded from the solid phase and accumulate in the liquid ahead of the interface. This accumulation generates steep concentration gradients, modifies local transport properties, and can drive secondary phenomena such as microphase separation, viscosity increases, and crystallization of secondary solutes. The distribution of solutes during freezing plays a central role in determining the composition and structure of the unfrozen regions, as well as the morphology and uniformity of the frozen phase.[12]

3.1. Concentration boundary layer and nonlinear diffusion

The accumulation of polymers ahead of the freezing front forms a concentration boundary layer whose structure and evolution play a central role in front morphology. As discussed in Section 2.1, this accumulation results from the imbalance between front advancement and polymer diffusion, captured by the Peclet number. When Pe > 1, advection dominates over diffusion, leading to steep gradients in local polymer concentration just ahead of the front.

These gradients are not static. In polymer solutions, the diffusivity D decreases sharply with concentration,[105] following the scaling law in eqn (2). As polymer accumulates, D drops, which further steepens the gradient and causes the front to encounter increasingly viscous and poorly diffusing material. This positive feedback loop enhances solute retention and leads to a dynamically narrowing accumulation layer.[12]

The morphological implications of this feedback are significant. As $D(c)$ falls, the effective Peclet number rises during freezing, extending the region of constitutional undercooling ahead of the front and making it more susceptible to morphological instabilities. In directional freezing, this manifests as earlier onset of cellular or dendritic growth and a reduced characteristic spacing between lamellae.[16] High-molecular-weight polymers, with steeper $D(c)$ decay, exhibit these effects at lower concentrations than their low-molecular-weight counterparts.

Recent experiments using directional freezing of PVA solutions have confirmed this concentration-driven sharpening effect.[80,106] These results underscore that the evolving concentration boundary layer, and the nonlinear transport it induces, is a central driver of morphological instability.

3.2. Solute trapping and partitioning

During solidification, solute trapping refers to the incorporation of solute molecules into the solid phase despite thermodynamic exclusion.[107,108] In polymer solutions, this typically occurs when the freezing front moves rapidly enough that polymer chains are kinetically prevented from diffusing away in time.[57] Under these conditions, some fraction of the polymer becomes trapped within the solid ice matrix, leading to non-equilibrium partitioning.[12,109]

This behavior is commonly described using either sharp-interface models, which define a partition coefficient $k = C_s/C_l$ across a discontinuous interface,[110] or continuous trapping models, which allow for smooth concentration gradients governed by local front velocity and solute mobility.[111] In the limit of slow, near-equilibrium freezing, high-molecular weight polymers experience strong entropic and steric exclusion from the ice lattice, and the partition coefficient approaches zero.[112,113]

At higher front velocities, however, several studies report a modest increase in k, even for large polymers.[114,115] This apparent increase does not reflect a breakdown of exclusion mechanisms, but rather the onset of kinetic trapping: when

the interface advances faster than polymer chains can diffuse or relax, solutes are engulfed before exclusion can be completed. In this regime, partitioning becomes controlled by the ratio of interface velocity to polymer diffusivity rather than by equilibrium thermodynamics alone.

This interpretation is formalized in continuous solute trapping models, such as the Aziz–Kaplan framework,[116] which express the partition coefficient as a smooth function of the front velocity,

$$k(V) = \frac{k_0 + \frac{V}{V_D}}{1 + \frac{V}{V_D}} \quad (5)$$

where k_0 is the equilibrium partition coefficient and $V_D = D/\lambda$ is a characteristic diffusive speed, with D the solute diffusivity and λ a microscopic interface width. Although originally developed for metallic alloys, this framework has been widely adapted to soft and polymeric systems to capture non-equilibrium solute incorporation during rapid freezing.

Within this view, strong exclusion ($k \approx 0$) and velocity-induced trapping ($k > 0$) represent two limiting cases of the same underlying process, distinguished by the degree of timescale separation between front propagation and polymer transport. Accordingly, there is broad consensus that high–molecular weight polymers remain thermodynamically excluded from ice, while finite partitioning observed at high freezing rates reflects kinetic trapping rather than true incorporation into the ice lattice.

In multicomponent polymer solutions, differential partitioning becomes even more complex. Smaller additives (*e.g.*, cryoprotectants or salts) may be trapped preferentially over larger polymer chains, leading to local osmotic gradients or the formation of concentration inhomogeneities. This effect is particularly relevant in aqueous biphasic systems, where thermodynamic phase separation between polymers and salts can occur during freezing, leading to microdomains of varied solute composition and freezing point.[117]

Solute trapping also affects the mechanical and thermal properties of the solid phase. Trapped polymers can interfere with crystal alignment, induce amorphous inclusions, or reduce crystallinity. For instance, Li *et al.* showed that sucrose solutions exhibit dendritic inhibition of ice fronts due to solute retention and water activity depression.[118] Similarly, our recent study on the freezing of PVA droplets demonstrated that front morphology—and the eventual disappearance of the pointy tip at the top of the frozen droplet—was modulated by polymer concentration and freezing rate. We showed that solute retention above the overlap concentration c^* influenced both thermal behavior and the evolution of solid shape.[119]

These combined effects—solute rejection, partial trapping, and differential partitioning—can also induce osmotic stresses in the unfrozen region, leading to phase segregation or shell-like structures. Experimental slicing of frozen droplets showed that when freezing proceeds from the bottom upward, the polymer concentration is lower in the frozen bottom region and higher in the frozen top region. This gradient arises from kinetic trapping and directional solute displacement during front progression.[119] Such asymmetries are critical to account for when predicting morphology and transport post-freezing, especially for applications in cryopreservation, food science, and freeze-casting.[120]

3.3. Microphase separation and dynamic heterogeneity

When the polymer concentration near the interface exceeds the solubility limit or crosses a glass transition threshold, the unfrozen solution may undergo microphase separation.[121] The onset of vitrification near the freezing front occurs when the local polymer concentration becomes high enough to elevate the T_g of the unfrozen phase above the ambient or subzero temperature of the system.[122,123] This transition arrests chain mobility and can lead to the formation of glassy, polymer-rich domains,[109,124,125] adjacent to growing ice crystals. Such vitrified layers limit further solute redistribution and can trap concentration gradients, preserving heterogeneity established during early solidification. The T_g is highly sensitive to polymer chemistry, molecular weight, and local hydration, and thus provides a useful threshold for predicting when the system transitions from a fluid-like to a solid-like state in the unfrozen phase.

Experimental observations of vitrified chitosan-rich regions in frozen PVA–chitosan scaffolds confirm that exceeding the local glass transition threshold during freezing can inhibit pore coalescence and trap concentration heterogeneities,[74,126] in line with predicted T_g-dependent transport arrest.[125,127] These secondary structures often persist after freezing and can template the final material morphology, especially in applications involving freeze-drying or crosslinking post-solidification.

To illustrate this progression and its spatial heterogeneity, Fig. 4 presents a schematic of the polymer concentration profile along the freezing direction. Far from the front, the solution remains in the dilute regime ($c < c^*$), but as the interface advances, solute exclusion leads to steep concentration gradients, with regions near the front exceeding the entanglement threshold (c_e) or even crossing the vitrification line when $T < T_g(c)$. This evolving profile links the local thermodynamic state to mobility, viscoelasticity, and ultimately the morphology imprinted in the frozen material.

3.4. Experimental methods for tracking solute redistribution

Tracking how polymers redistribute during freezing is essential for linking interfacial transport to final material structure. However, the rapid timescales, steep concentration gradients, and cryogenic conditions make direct measurement challenging. Techniques to probe solute behavior fall broadly into three categories: optical/spectroscopic mapping, cryo-imaging of quenched structures, and microfluidic model systems.

Label-based fluorescence microscopy remains one of the most accessible approaches.[94,128,129] Polymers are covalently tagged with dyes, or dyes that partition with the polymer-rich phase are added,[130] enabling time-resolved imaging of exclusion and boundary layer formation. Confocal setups can resolve gradients with micron resolution, while cryo-confocal

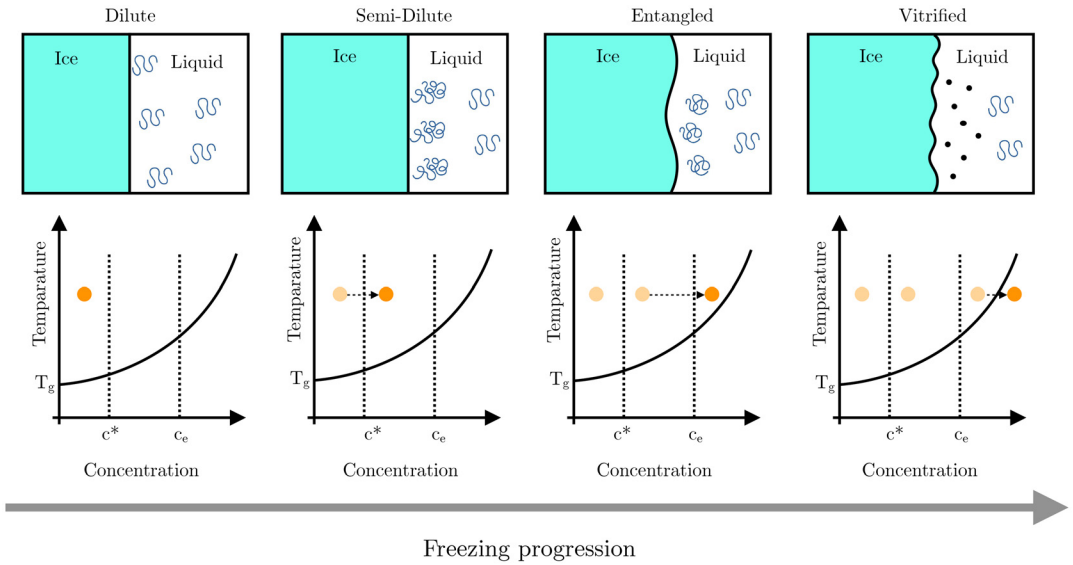

Fig. 4 Schematic of concentration evolution and state transitions during directional freezing of a polymer solution. As the ice front advances (arrow of time, left to right), excluded polymer chains accumulate in a boundary layer whose concentration increases from the dilute regime ($c < c^*$) far from the front, through the semi-dilute regime ($c^* < c < c_e$), and into the entangled regime ($c > c_e$) near the interface. The overlap concentration c^* and entanglement concentrations c_e are indicated by vertical dashed lines. Local concentration buildup is spatially heterogeneous: regions near the front approach vitrification when the glass transition temperature $T_g(c)$ exceeds the local temperature, while more distant regions remain fluid and dilute. This spatial variation in concentration and rheology influences diffusion, viscoelasticity, and the stability of the freezing front.

platforms combine rapid cooling with temperature-controlled objectives to capture front progression and solute enrichment in real time.[131]

Label-free chemical mapping is possible *via* Raman[132,133] or coherent anti-Stokes Raman scattering (CARS) microscopy,[134,135] which exploit vibrational fingerprints to differentiate polymer-rich and water-rich domains. These methods reveal concentration fields without perturbing the chemistry, albeit with slower acquisition and greater sensitivity to sample heterogeneity. High-speed CARS platforms are beginning to bridge this trade-off by enabling rapid, label-free vibrational contrast, thereby reducing perturbations to polymer–ice interactions while approaching the temporal resolution required to capture fast freezing dynamics.[136,137]

Post-freezing characterization relies heavily on cryo-scanning electron microscopy (cryo-SEM), which visualizes microstructure after quenching.[138] When paired with energy-dispersive X-ray spectroscopy (EDX), cryo-SEM can detect compositional heterogeneities indirectly *via* pore morphology or elemental mapping.[8,139,140] Freeze-fracture or cryo-slicing provides spatial concentration profiles in layered microstructures, useful for systems with shell formation or radial segregation.[141]

Synchrotron-based cryo-tomography has emerged as a powerful 3D imaging tool, reconstructing internal solute-rich domains at submicron resolution.[142–145] Microfluidic freezing platforms complement these techniques by providing optical access, precise thermal control, and tunable flow geometries, enabling systematic tests of diffusion–advection models under well-defined gradients.

Strong scattering, refractive-index mismatch, and moving phase boundaries in multiphase or phase-separated systems substantially limit the utility of optical methods that perform well in homogeneous solutions.[146] In highly viscous or polymer-rich boundary layers, probe mobility is strongly reduced and fluorescence recovery becomes unreliable, complicating quantitative interpretation. Label-free vibrational techniques mitigate chemical perturbation but remain challenged by signal attenuation, slow acquisition, and loss of contrast in optically dense or glassy regions.

Higher-resolution approaches such as cryo-SEM or cryo-tomography provide detailed post-freezing snapshots, but are inherently unable to resolve transient solute redistribution during front propagation. As a result, characterizing solute dynamics in multiphase or high-viscosity polymer systems remains constrained by the lack of techniques that simultaneously offer non-invasiveness, temporal resolution, and penetration depth across heterogeneous freezing environments.[147]

Together, these methods are beginning to resolve the spatial and temporal complexity of solute redistribution during freezing, supplying the quantitative concentration maps needed to parameterize and validate coupled transport models.

4. Freezing front morphology and stability

The morphology of the solidification front plays a central role in determining the spatial organization and heterogeneity of

the frozen polymer solution. As the ice front advances, its shape and stability are governed by the interplay between thermal gradients, solute rejection, interfacial adsorption, and the transport properties of the surrounding solution. These factors collectively define whether the front remains planar or becomes unstable, giving rise to cellular, lamellar, or dendritic growth patterns.[78,127]

4.1. Planar, cellular, and dendritic fronts

The transition from planar to cellular or dendritic ice fronts in polymer solutions is a hallmark of morphological instability driven by solute accumulation.[4,47] When exclusion layers build up ahead of the front, local undercooling increases until perturbations are amplified.[148,149]

This transition is well described by the Mullins–Sekerka analysis, which predicts that a planar front is unstable when the thermal gradient in the liquid ahead of the interface falls below a critical value determined by solute accumulation:

$$\frac{\partial T}{\partial x} < \frac{mC_0(1-k)}{D} \quad (6)$$

where m is the slope of the liquidus line, C_0 is the initial solute concentration, k is the equilibrium partition coefficient, and D is the solute diffusivity.[150] This expression captures how reduced diffusivity or increased solute rejection—both typical in polymer solutions—can destabilize the interface by amplifying perturbations in the temperature or concentration field.

In salt solutions, this classical picture is often a good first-order description: ions remain highly mobile, partitioning is largely governed by colligative thermodynamics, and cellular or mushy morphologies can frequently be rationalized using diffusion-controlled models with interfacial corrections.[13–15] Polymer solutions, in contrast, can violate these assumptions because the accumulation layer may become highly viscous or even glassy, and polymer–ice interactions (adsorption, pinning, bound water) can directly perturb local growth kinetics.

These differences are evident in direct comparisons between NaCl and PVA solutions under unidirectional freezing (Fig. 4a).[12] While NaCl shows localized perturbations consistent with Mullins–Sekerka-type behavior, PVA exhibits global front destabilization from the onset. This behavior has been attributed to the low diffusivity and strong adsorption of polymer chains, which rapidly generate steep concentration gradients and microscale pinning sites. Beyond front shape, solute accumulation can induce phase separation or trapping near the interface, modifying both the morphology and composition of the frozen phase.[151] These effects are coupled to the front's thermal and solutal environment, as seen in directional freezing of PEG–protein solutions and collagen scaffolds, where changes in freezing rate or polymer loading shift front morphology and pore architecture (Fig. 4b and c).[127,152,153] Simulations of poly(vinyl alcohol) (PVA) interacting with ice further reveal that slow surface coverage can delay uniform growth inhibition and generate heterogeneous freezing dynamics.[65,154] Consistent with this, directional freezing of PVA–chitosan blends shows morphological transitions from planar to cellular fronts as polymer concentration or freezing rate is varied.[127]

4.2. Influence of polymer properties on front shape

The morphology of the ice front is sensitive to the physical characteristics of the polymer solution, including molecular weight, chain stiffness, and polymer architecture. These properties shape the evolution of the solid–liquid interface by modifying both the structure of the exclusion layer and the stability of growing facets.

Solutions containing high-molecular-weight or branched polymers often develop steeper concentration gradients, due to reduced diffusivity and slower chain relaxation.[155] These steep gradients enhance constitutional undercooling and increase the likelihood of front destabilization. Under directional freezing, this effect manifests as more frequent transitions from planar to cellular growth and narrower lamellar spacing.[79]

The stiffness of the polymer chain modulates how excluded solutes interact with the moving front.[154,156] Flexible coils such as PEG or PVA tend to conform to local flow and accumulate isotropically. In contrast, semi-rigid or extended chains—such as chitosan or xanthan—may align preferentially near the interface and introduce anisotropy in solute buildup.[157] This alignment can bias the orientation of lamellae or induce lateral asymmetries in the front.

Polymer conformation also influences front pinning. Flexible chains more readily deform around protrusions, while stiffer chains resist compression and promote the formation of stable asperities. These effects are amplified in confined geometries, where steric interactions with channel walls or droplet curvature constrain chain mobility and further shape front evolution.[100]

Front morphology is additionally impacted by rheological thresholds. As concentration increases, transitions from dilute to semi-dilute or entangled regimes suppress chain mobility and modify local viscosity.[158] These rheological changes contribute to abrupt shifts in lamellar symmetry, tip-splitting behavior, and pore alignment. In multicomponent systems, where polymers of different flexibility coexist, this effect can lead to compositional banding or phase-coupled morphological transitions.[159]

The physical imprint of polymer properties on the freezing front is thus expressed through a variety of shape outcomes: broadened or narrowed lamellae, directional tilting, tip sharpening or splitting, and front symmetry breaking. These morphological signatures offer a potential route to infer local polymer behavior from frozen structure and to tune solidification pathways through polymer design.

4.3. Geometric confinement and boundary conditions

At macroscopic scales, the morphology and stability of the freezing front are strongly influenced by the geometry of the domain and the boundary conditions imposed by its surroundings. Confinement in droplets, capillaries, thin films, or

microfluidic channels[160] reshapes the thermal and solutal fields, altering interfacial dynamics relative to bulk freezing.[16]

In small or curved domains, boundary-induced thermal gradients modify local undercooling *via* the Gibbs–Thomson effect. For example, in droplets the ice front often adopts a curved profile, with growth favored at the apex or edges depending on heat extraction pathways.[119] In planar Hele–Shaw cells or thin films, the front is laterally constrained, which can enforce directional growth and bias lamellar alignment.[45,155] Confinement also limits lateral solute redistribution. In narrow geometries, excluded polymers cannot diffuse far from the freezing interface, which enhances solute crowding and promotes earlier onset of phase separation or vitrification compared to unbounded systems. The restriction of convective flows simplifies the transport field, enabling diffusion-dominated regimes to be studied in isolation.[47,161]

Macrogeometry influences instability selection as well. In bulk, the wavelength of cellular or dendritic perturbations is determined by a balance of solutal and thermal diffusivities, interface velocity, and interfacial energy.[19,37,77] In confined domains, the available space can suppress long-wavelength modes, stabilize otherwise unstable fronts, or enforce symmetry breaking through wall effects.[162] For example, lamella spacing may be pinned by the channel width, or cellular fronts may be entirely suppressed in capillaries narrower than the critical instability wavelength.[163]

Boundary surface properties, such as wettability, roughness, and thermal conductivity, further control nucleation and growth pathways.[164–166] Preferential wetting can seed ice at specific locations, while thermal contrasts between walls and liquid can guide front direction or velocity. In droplets on solid supports, thermocapillary flows induced by surface temperature gradients can redistribute solutes and modify front shape near the contact line.[79,119,167]

Observing solute distribution under irregular or asymmetric geometric constraints remains a major experimental bottleneck. Most existing characterization techniques are optimized for regular, optically accessible geometries (*e.g.*, planar cells or cylindrical channels) and do not readily extend to porous media or biological tissues. Confocal microscopy can capture transport in transparent systems, but loses resolution and quantitative reliability in highly scattering, heterogeneous, or tortuous environments.[32] Cryo-SEM and related approaches (sectioning, freeze-fracture) provide high-resolution spatial snapshots of complex structures, yet are inherently post-mortem and cannot resolve transient solute transport during front propagation. X-ray and synchrotron-based tomography offer three-dimensional access to irregular architectures, but typically at reduced temporal resolution and limited chemical specificity.[168] As a result, existing techniques provide complementary but incomplete views, and no single method currently meets the combined requirements of non-invasiveness, temporal resolution, and geometric generality needed to fully characterize solute transport in irregular or tissue-like freezing environments.[169]

In summary, macro-scale confinement and boundary effects determine how heat and solutes are transported to and from the freezing front, constrain the available instability modes, and bias the selection of morphological patterns. These effects operate in parallel with polymer-scale confinement (Section 2.3) but act over larger length scales, setting global constraints within which local interfacial dynamics unfold.

4.4. Experimental observations and visualization methods

Observing freezing front morphology in polymer solutions requires techniques that resolve interface shape, dynamics, and defect evolution across relevant length scales. The most common post-mortem method is cryogenic scanning electron microscopy (cryo-SEM), which reveals pore architecture, lamellar alignment, and interfacial roughness after ice sublimation.[170] Applied to directionally frozen samples, cryo-SEM quantifies lamella spacing and anisotropy as functions of cooling rate, polymer content, or additive chemistry.

For dynamic observation, thin-film and Hele–Shaw geometries allow brightfield or phase-contrast microscopy of front motion under controlled temperature gradients. These optical setups can capture the onset of instabilities—such as tip-splitting, sidebranching, and lamella competition—while correlating them with imposed thermal or solutal conditions.[32,119,171] Incorporating fluorescence labeling enables simultaneous visualization of front morphology and local solute enrichment, bridging Sections 3.4 and 4.4 in scope.[107,129]

X-ray phase contrast imaging and micro-computed tomography (μCT) offer non-destructive 3D reconstructions of frozen or freeze-dried structures, including pore connectivity and anisotropy.[172,173] Synchrotron-based implementations achieve the temporal resolution needed to track front motion in opaque systems,[145] although contrast for soft polymers remains a challenge.

Spectroscopic approaches such as Fourier-transform infrared (FTIR) or Raman microscopy can be combined with imaging to relate morphology to local composition, for example by mapping hydration state or secondary phase formation *in situ*.[174,175]

Emerging methods target mechanical and transport properties at the interface: Brillouin microscopy measures local viscoelasticity, while cryo-focused ion beam (cryo-FIB) milling allows site-specific cross-sectioning of features such as lamella tips or branching points.[176] These tools, when integrated with microfluidic freezing cells, offer a path toward real-time, high-resolution mapping of both shape evolution and underlying physical drivers.

By pairing structural visualization with concurrent measurement of thermal and solutal fields, these methods enable a more complete understanding of how polymer chemistry and processing conditions shape the freezing front.

5. Modeling approaches and multiscale coupling

Modeling the freezing of polymer solutions requires capturing phenomena that span multiple spatial and temporal scales,

from molecular interactions at the ice interface to large-scale morphological evolution. These processes are strongly coupled: interfacial adsorption, solute rejection, and phase boundary motion all feed back into one another. Over the past two decades, a combination of theoretical, computational, and empirical modeling strategies has been developed to address this complexity.[58] This section outlines key modeling frameworks that have advanced our understanding of polymer solution freezing and highlights opportunities for bridging scales.

5.1. Molecular simulations of polymer–ice interfaces

Molecular dynamics (MD) simulations offer unique insight into the nanoscale interactions between polymers and ice surfaces, often challenging to access experimentally. These simulations reveal how polymer chemistry, chain length, and flexibility control adsorption kinetics, interfacial energy, and local freezing behavior.

For poly(vinyl alcohol) (PVA), simulations show selective and persistent binding to prismatic ice faces, stabilized by hydrogen bonding between hydroxyl groups and the ice lattice.[18,65,154] However, despite strong binding affinity, surface coverage increases slowly over time. This slow propagation of adsorption is attributed to kinetic barriers rather than weak interaction energy. Naullage and Molinero demonstrated that individual PVA chains adsorb rapidly, but the spreading of adsorbed chains across the surface is hindered by entropic constraints and site-specific alignment requirements. As a result, even at high bulk concentrations, ice surfaces remain partially covered, limiting the effectiveness of growth inhibition.

These simulations clarify why polymers like PVA show sublinear increases in ice recrystallization inhibition (IRI) with concentration.[177,178] Unlike antifreeze proteins, which bind irreversibly to lattice-specific sites and halt front advance, polymers engage in reversible, kinetically constrained adsorption. The distinction between adsorption energy and adsorption dynamics emerges as a key factor in determining how polymers modulate freezing.

MD simulations also permit atomistic comparison of different polymer chemistries.[68,179] For instance, polyethylene glycol (PEG) interacts weakly with ice (Fig. 6), displaying minimal residence time and low surface affinity, consistent with its poor performance as an IRI agent.[180,181] Variants in chain architecture, such as branching or copolymerization, can further modulate adsorption behavior, offering design parameters for tuning interfacial effects.

Beyond binding, simulations capture how polymers deform near the interface. Flexible chains tend to flatten and align along the surface, while stiffer chains maintain more coiled or looping conformations.[177,180,182] These geometries influence the density of contacts with the ice lattice and the degree of interfacial roughening. The presence of adsorbed polymers alters water structuring near the surface, locally disrupting hydrogen bonding and reducing crystal growth velocity.[106,154]

Together, molecular simulations provide mechanistic understanding of how polymers influence interfacial freezing through a combination of adsorption thermodynamics, chain conformation, and kinetic constraints. They complement experimental efforts by revealing transient, spatially heterogeneous phenomena that govern early-stage solidification.[183]

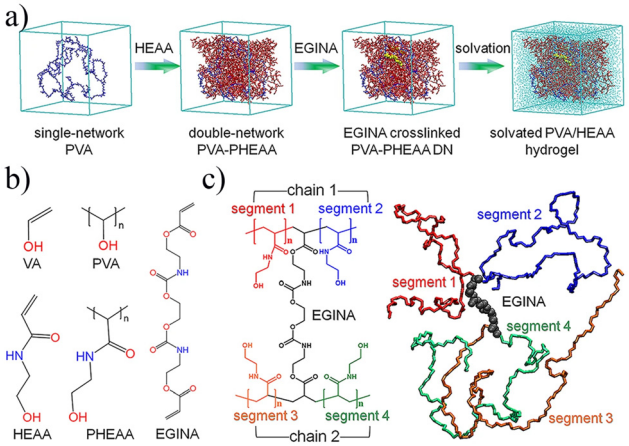

Fig. 6 Multiscale construction of crosslinked hydrogel networks for molecular simulations. (a) Stepwise modelling pipeline to build solvated double-network hydrogels from monomer structures and crosslinkers. (b and c) Molecular structures and 3D representations of the polymer chains and EGINA crosslinking topology. Adapted from Liu *et al.*[193]

5.2. Continuum transport and front coupled models

At the mesoscale, the dynamics of solute redistribution and front motion are often captured using coupled transport equations that account for mass conservation, thermal diffusion, and interface kinetics.[112,184] The Stefan problem provides a classical framework for modeling front motion under freezing, but must be extended to incorporate concentration-dependent diffusivity, viscosity, and solute exclusion.

Phase-field models are particularly well-suited for simulating complex front morphologies in multicomponent systems.[109] These models treat the solid–liquid interface as a diffuse boundary and can incorporate realistic thermodynamic free energy landscapes and kinetic asymmetries.[12] In polymer solutions, phase-field approaches have been adapted to capture how solute accumulation, viscosity gradients, and interfacial energy anisotropy influence front branching, lamellar alignment, or cellular instabilities.[109]

Experimental observations of anisotropic pore formation in systems such as PVA–chitosan blends and polymer–nanoparticle composites offer critical benchmarks for these models.[185–187] For instance, directional freezing of PVA–chitosan solutions under controlled gradients produces morphologies that reflect both phase segregation and dynamic polymer retention, with pore alignment and spacing varying as a function of composition and freezing rate.[127] Similarly, Lee *et al.*[188] reported transitions from planar to dendritic morphologies in freeze-cast PVDF–SiO_2 and HPC–SiO_2 systems as a function of cooling rate and filler content. At high freezing rates, lamellar spacing decreased and ice front branching

intensified, consistent with phase-field predictions of constitutional undercooling and tip-splitting.

These experiments also suggest empirical scaling laws that connect process conditions to front structure. Lee *et al.* proposed a relationship of the form:

$$L = (8D\Delta T)^{0.5} F^{-0.5} \quad (7)$$

where L is the characteristic lamellar spacing, D the solute diffusivity, ΔT the temperature gradient, and F the freezing rate.[188] Such expressions complement computational approaches by providing parameterized inputs and scaling benchmarks for model calibration. Moreover, the presence of composite additives and the resulting phase segregation highlight the need for models that incorporate multicomponent transport, polymer–additive interactions, and time-dependent changes in rheology.[189]

Together, these findings reinforce the value of integrating continuum modeling with well-characterized directional freezing experiments to develop predictive frameworks for morphology control in polymer solution solidification.

5.3. Linking scales: from molecular to macroscopic behaviors

Capturing the freezing of polymer solutions requires frameworks that bridge molecular-scale interfacial processes and the emergent macroscopic morphologies. While molecular simulations provide detailed insight into polymer adsorption, exclusion, and chain conformations near ice surfaces, these results must be translated into effective parameters that inform continuum-level models. One approach is to extract interfacial thermodynamic quantities such as surface energy modifications, adsorption affinities, or ice binding propensities from simulations and incorporate them into phase-field or front-tracking models as boundary conditions or free energy terms.[190–192]

Multiscale strategies have been developed to link polymer chemistry, network structure, and macroscale behavior.[109] In systems where network formation occurs concurrently with freezing, hybrid modeling platforms have combined coarse-grained random walk algorithms with reactive kinetics to generate polymer architectures that reflect experimentally observed topologies (Fig. 5).[193] These methods allow emergent structural features such as connectivity, pore distribution, and anisotropy to be predicted directly from monomer-level rules, offering a bridge between reaction chemistry, interfacial physics, and bulk mechanics.[193]

Such hybrid models complement molecular dynamics or dissipative particle dynamics simulations by extending accessible timescales and domain sizes. In freezing systems, this allows the incorporation of realistic polymer microstructure, including loop formation, network defects, and entanglement density, into predictive models of pore formation and transport. As a result, continuum models that simulate front morphology can be enhanced with polymer-specific rheology and elasticity derived from the underlying chain dynamics.[194,195]

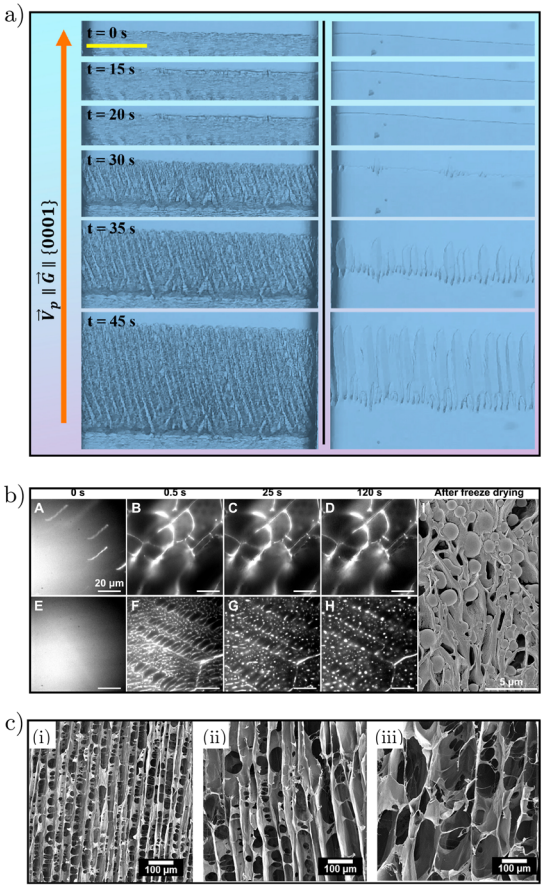

Fig. 5 Interplay between front stability, solute redistribution, and resulting morphology in unidirectional freezing of polymer solutions. (a) *In situ* visualization of morphological instability during unidirectional freezing of a polymer solution (left) and a salt solution (right) under identical thermal gradients. The PVA solution exhibits immediate global front perturbations due to low diffusivity and polymer-specific interactions, while NaCl displays localized instability consistent with classical Mullins–Sekerka behavior. Figure reproduced from Zhang *et al.*,[12] with permission from Elsevier copyright 2021. (b) Real-time TIRF microscopy images showing freezing-induced phase separation in PEG–BSA solutions, alongside SEM of the final lyophilized scaffold. Adapted from Song *et al.*[127] (c) SEM micrographs showing vertical cross-sections of unidirectionally frozen collagen scaffolds at decreasing cooling rates. Lamellar spacing increases and bridging decreases with lower gradients, indicating enhanced front stability. Figure reproduced from Divakar *et al.*, with permission from Elsevier, copyright 2019.[153]

5.4. Implications for applications and materials design

The interfacial mechanisms reviewed here have direct implications for a wide range of technologies that rely on controlled freezing of polymer-containing systems. In cryogel fabrication and freeze-casting, for example, polymer exclusion, crowding, and rheological arrest govern pore size, connectivity, and anisotropy.[3,74,185,186,196] Operating in diffusion-dominated regimes favors well-defined lamellar or cellular architectures, while viscous or vitrification-dominated regimes suppress mass redistribution and lead to more homogeneous or arrested microstructures.[12,197] The regime map summarized in

Fig. 3 provides a conceptual framework for selecting polymer concentration and thermal driving to access desired structural outcomes without relying solely on trial-and-error processing.

In cryopreservation and biological freezing, polymer–ice interactions at the nanoscale critically influence cell survival and biomolecular integrity.[1,26,41,198] Accumulation-induced freezing point depression and interfacial adsorption can locally reduce ice growth rates and mitigate mechanical damage, whereas excessive crowding or vitrification may trap solutes and generate steep chemical gradients.[32,97,199] Understanding where a given system lies within the transport–thermodynamic regimes identified here helps rationalize the distinct roles of penetrating and non-penetrating cryoprotectants, as well as the transition between controlled ice formation and vitrified states.

Food and soft-matter systems provide another important class of applications in which polymer-controlled freezing determines texture, stability, and shelf life.[7,68,109,121,200] Polysaccharides and proteins are often introduced to modulate ice crystal size and inhibit recrystallization, effects that arise from the same exclusion, adsorption, and rheological mechanisms discussed throughout this review.[17,122,201] Framing these effects within a unified regime map highlights how modest changes in concentration or cooling rate can shift systems between diffusion-controlled smoothing, interfacial pinning, and kinetic arrest, thereby offering physically grounded guidelines for formulation and processing.

More broadly, the framework developed here emphasizes that freezing of polymer solutions cannot be optimized by thermal control alone. Instead, functional performance emerges from the coupled interplay of polymer physics, interfacial energetics, and transport processes at the freezing front. By situating specific applications within the broader parameter space of polymer concentration and thermal driving, this review provides a basis for translating nanoscale interfacial mechanisms into predictive design rules for freezing-based technologies.

5.5. Open questions in model fidelity and predictive design

Despite significant progress, existing models remain limited in capturing the full complexity of polymer solution freezing. Many models assume dilute or ideal polymer behavior and neglect chain entanglement, elasticity, or multicomponent coupling.[12,122] Thermophysical properties such as diffusivity, viscosity, or interfacial energy are often assumed constant or weakly dependent on concentration, limiting the accuracy of simulations at high polymer content.

Improving predictive capabilities will require experimental input on key parameters under freezing conditions, including dynamic measurements of viscosity, diffusivity, and interfacial structure. It will also benefit from new model formulations that incorporate polymer conformational entropy, concentration-dependent elasticity, and interfacial adsorption in a unified framework.[202]

6. Outlook and open questions

The freezing of polymer solutions is governed by a rich interplay of interfacial interactions, solute dynamics, and morphological evolution. While progress has been made in characterizing individual mechanisms such as polymer rejection[24,203] interface adsorption,[11,62,180] or front instabilities,[32,37,148] an integrated framework that connects these processes across scales is still emerging. The complexity of these systems, rooted in their molecular heterogeneity and strong coupling between transport, mechanics, and thermodynamics, presents both a challenge and an opportunity for the development of predictive models and materials-by-design strategies.

Several open questions remain. First, the physical basis for polymer–ice interactions is not yet fully understood. While molecular simulations and cryo-imaging suggest that adsorption and pinning can significantly alter front dynamics, quantitative measurements of interfacial energy, binding strength, or residence time under dynamic freezing conditions are scarce. Further work is needed to characterize how polymer chemistry, chain stiffness, and solution structure control interfacial behavior.

Second, solute redistribution near the freezing front is often treated as a purely diffusive or advection-driven process, but real systems exhibit strong concentration dependence, feedback from local viscosity, and non-equilibrium trapping. More refined transport models that account for viscoelastic effects, crowding, and local confinement could improve the accuracy of front predictions, especially in high-concentration regimes.

Third, most current models treat the polymer solution as a passive background medium, rather than an active, deformable material. Incorporating polymer chain elasticity, conformational entropy, and poroelastic feedback into solidification models may open new perspectives, particularly in confined geometries or during rapid freezing.

Finally, the integration of experimental and computational approaches remains a central goal. High-resolution, time-resolved imaging of freezing fronts, coupled with concentration mapping and local mechanical measurements, would provide the data needed to calibrate and validate multiscale models. Advances in machine learning and data-driven modeling may help link simulation outputs and experimental observations to final material morphology.

Looking forward, the study of polymer solution freezing offers a valuable testbed for understanding coupled interfacial phenomena in soft matter. Beyond its relevance for cryogels and porous materials, it touches on fundamental questions in phase transitions, non-equilibrium thermodynamics, and transport in complex fluids. Addressing these open problems will require continued dialogue between theory, simulation, and experiment, and may enable new classes of structured materials designed through controlled solidification.

Author contributions

NU and JFL wrote the manuscript. JFL supervised the overall project.

Conflicts of interest

There are no conflicts to declare.

Data availability

No new data has been generated.

Acknowledgements

This work was supported by the ACS PRF DNI grant #67719-DNI7.

References

1 Z. Liu, X. Zheng and J. Wang, Bioinspired ice-binding materials for tissue and organ cryopreservation, *J. Am. Chem. Soc.*, 2022, **144**, 5685–5701.
2 X. Zhang, H. Qi, J. Yang, X. Chen and L. Zhang, Development of low immunogenic antifreeze peptides for cryopreservation, *Ind. Eng. Chem. Res.*, 2023, **62**, 12063–12072.
3 S. Jiang, *et al.*, Cryoprotectant enables structural control of porous scaffolds for exploration of cellular mechano-responsiveness in 3D, *Nat. Commun.*, 2019, **10**, 3491.
4 J. Wu, Q. Zhao, J. Sun and Q. Zhou, Preparation of poly (ethylene glycol) aligned porous cryogels using a unidirectional freezing technique, *Soft Matter*, 2012, **8**, 3620–3626.
5 M. C. Gutiérrez, *et al.*, Poly (vinyl alcohol) scaffolds with tailored morphologies for drug delivery and controlled release, *Adv. Funct. Mater.*, 2007, **17**, 3505–3513.
6 D. E. Mitchell, *et al.*, Ice-recrystallization inhibiting polymers protect proteins against freeze-stress and enable glycerol-free cryostorage, *Mater. Horiz.*, 2019, **6**, 364–368.
7 G. Jia, Y. Chen, A. Sun and V. Orlien, Control of ice crystal nucleation and growth during the food freezing process, *Compr. Rev. Food Sci. Food Saf.*, 2022, **21**, 2433–2454.
8 H. Joukhdar, *et al.*, Imparting multi-scalar architectural control into silk materials using a simple multi-functional ice-templating fabrication platform, *Adv. Mater. Technol.*, 2023, **8**, 2201642.
9 K. Izutsu, *et al.*, Application of the Thermal Analysis of Frozen Aqueous Solutions to Assess the Miscibility of Hyaluronic Acid and Polymers Used for Dissolving Microneedles, *Pharmaceutics*, 2024, **16**, 1280.
10 M. R. Kim, H. J. Park, K. H. Cheon, C. K. Yeom and K. Y. Lee, Novel behavior in a polymer solution: the disappearance of the melting temperature (Tm) and enthalpy change (ΔHm) of the solvent, *Sci. Rep.*, 2020, **10**, 13348.
11 K. Yin, *et al.*, Hierarchical structure formation by crystal growth-front instabilities during ice templating, *Proc. Natl. Acad. Sci. U. S. A.*, 2023, **120**, e2210242120.
12 T. Zhang, X. Xu, Z. Yuan and Q. Li, The planar instability during unidirectional freezing of a macromolecular polymer solution: Diffusion-controlled or not?, *Phys. Rev. B: Condens. Matter Mater. Phys.*, 2021, **608**, 412875.
13 F. Chu, *et al.*, Interfacial ice sprouting during salty water droplet freezing, *Nat. Commun.*, 2024, **15**, 2249.
14 C. Zhao, Y. Lin, X. Wu, X. Zhang and F. Chu, Nanoscale insights on the freezing front propagation and ion behaviors during seawater freezing, *Appl. Surf. Sci.*, 2023, **641**, 158499.
15 X. Lin, C. Zhang, S. Hu and R. Chen, Heterogeneous ice nucleation of salt solution in porous media, *J. Chem. Phys.*, 2024, **160**, 094501.
16 M. A. Rodrigues, M. A. Miller, M. A. Glass, S. K. Singh and K. P. Johnston, Effect of freezing rate and dendritic ice formation on concentration profiles of proteins frozen in cylindrical vessels, *J. Pharm. Sci.*, 2011, **100**, 1316–1329.
17 A. E. R. Fayter, M. Hasan, T. R. Congdon, I. Kontopoulou and M. I. Gibson, Ice recrystallisation inhibiting polymers prevent irreversible protein aggregation during solvent-free cryopreservation as additives and as covalent polymer-protein conjugates, *Eur. Polym. J.*, 2020, **140**, 110036.
18 M. Bhendale, A. Indra and J. K. Singh, Does freezing induce self-assembly of polymers? A molecular dynamics study, *Soft Matter*, 2023, **19**, 7570–7579.
19 M. F. Butler, Freeze concentration of solutes at the ice/solution interface studied by optical interferometry, *Cryst. Growth Des.*, 2002, **2**, 541–548.
20 R. Mastrangelo, *et al.*, Twin-Chain cryogels: probing the nanostructure evolution at freezing through Small Angle Neutron Scattering, *J. Colloid Interface Sci.*, 2025, 139213.
21 K. Izutsu and K. Shigeo, Phase separation of polyelectrolytes and non-ionic polymers in frozen solutions, *Phys. Chem. Chem. Phys.*, 2000, **2**, 123–127.
22 R. M. Reddy, A. Srivastava and A. Kumar, Monosaccharide-responsive phenylboronate-polyol cell scaffolds for cell sheet and tissue engineering applications, *PLoS One*, 2013, **8**, e77861.
23 H. Schoof, J. Apel, I. Heschel and G. Rau, Control of pore structure and size in freeze-dried collagen sponges, *J. Biomed. Mater. Res.*, 2001, **58**, 352–357.
24 G. Petzold and J. M. Aguilera, Ice morphology: fundamentals and technological applications in foods, *Food Biophys.*, 2009, **4**, 378–396.
25 Y. Suzuki, Polymerization-induced vitrification, apparent phase separation, and reaction acceleration during bulk polymerization, *Polym. J.*, 2023, **55**, 807–815.
26 K. Matsumura, F. Hayashi, T. Nagashima, R. Rajan and S.-H. Hyon, Molecular mechanisms of cell cryopreserva-

tion with polyampholytes studied by solid-state NMR, *Commun. Mater.*, 2021, **2**, 15.
27 A. A. Burkey, C. L. Riley, L. K. Wang, T. A. Hatridge and N. A. Lynd, Understanding poly (vinyl alcohol)-mediated ice recrystallization inhibition through ice adsorption measurement and pH effects, *Biomacromolecules*, 2018, **19**, 248–255.
28 N. Baccile, G. B. Messaoud, T. Zinn and F. M. Fernandes, Soft lamellar solid foams from ice-templating of self-assembled lipid hydrogels: organization drives the mechanical properties, *Mater. Horiz.*, 2019, **6**, 2073–2086.
29 A. Seifert, J. Gruber, U. Gbureck and J. Groll, Morphological control of freeze-structured scaffolds by selective temperature and material control in the ice-templating process, *Adv. Eng. Mater.*, 2022, **24**, 2100860.
30 S. Samitsu, *et al.*, Flash freezing route to mesoporous polymer nanofibre networks, *Nat. Commun.*, 2013, **4**, 2653.
31 J. Wu, *et al.*, Asymmetric Aramid Aerogel Composite with Durable and Covert Thermal Management via Janus Heat Transfer Structure, *Nano Lett.*, 2024, **24**, 14020–14027.
32 D. Dedovets, C. Monteux and S. Deville, Five-dimensional imaging of freezing emulsions with solute effects, *Science*, 2018, **360**, 303–306.
33 D. Dedovets and S. Deville, Multiphase imaging of freezing particle suspensions by confocal microscopy, *J. Eur. Ceram. Soc.*, 2018, **38**, 2687–2693.
34 J. M. Pardo, E. Moya-Albor, G. Ortega-Ibarra and J. Brieva, Freezing front velocity estimation using image processing techniques, *Measurement*, 2020, **151**, 107085.
35 A. E. Donius, *et al.*, Cryogenic EBSD reveals structure of directionally solidified ice–polymer composite, *Mater. Charact.*, 2014, **93**, 184–190.
36 P. A. Albouy, *et al.*, Freezing-induced self-assembly of amphiphilic molecules, *Soft Matter*, 2017, **13**, 1759–1763.
37 S. Deville, *et al.*, Metastable and unstable cellular solidification of colloidal suspensions, *Nat. Mater.*, 2009, **8**, 966–972.
38 T. Vogel, M. Bachmann and W. Janke, Freezing and collapse of flexible polymers, *arXiv*, 2009, preprint, arXiv:0902.2340, DOI: 10.48550/arXiv.0902.2340.
39 T. Sato, I. Yasuda, N. Arai and K. Yasuoka, Molecular Dynamics Investigation of Static and Dynamic Interfacial Properties in Ice-Polymer Premelting Layers, *arXiv*, 2025, preprint, arXiv:2504.19628, DOI: 10.48550/arXiv.2504.19628.
40 P. M. Naullage, Y. Qiu and V. Molinero, What controls the limit of supercooling and superheating of pinned ice surfaces?, *J. Phys. Chem. Lett.*, 2018, **9**, 1712–1720.
41 U. G. K. Wegst, M. Schecter, A. E. Donius and P. M. Hunger, Biomaterials by freeze casting, *Philos. Trans. R. Soc., A*, 2010, **368**, 2099–2121.
42 H. Zhang and A. I. Cooper, Aligned porous structures by directional freezing, *Adv. Mater.*, 2007, **19**, 1529–1533.
43 H. Joukhdar, *et al.*, Ice templating soft matter: fundamental principles and fabrication approaches to tailor pore structure and morphology and their biomedical applications, *Adv. Mater.*, 2021, **33**, 2100091.
44 W. Kurz, D. Fisher and M. Rappaz, in *Fundamentals of solidification*, 2023.
45 L. Wang, J. You, Z. Wang, J. Wang and X. Lin, Interface instability modes in freezing colloidal suspensions: revealed from onset of planar instability, *Sci. Rep.*, 2016, **6**, 23358.
46 J. You, *et al.*, Dynamic particle packing in freezing colloidal suspensions, *Colloids Surf., A*, 2017, **531**, 93–98.
47 M. F. Butler, Instability formation and directional dendritic growth of ice studied by optical interferometry, *Cryst. Growth Des.*, 2001, **1**, 213–223.
48 W. W. Graessley, Polymer chain dimensions and the dependence of viscoelastic properties on concentration, molecular weight and solvent power, *Polymer*, 1980, **21**, 258–262.
49 P.-G. De Gennes, *Scaling Concepts in Polymer Physics*, Cornell University Press, 1979.
50 H. Hervet, L. Leger and F. Rondelez, Self-diffusion in polymer solutions: a test for scaling and reptation, *Phys. Rev. Lett.*, 1979, **42**, 1681.
51 S. Mariya, J. J. Barr, P. Sunthar and J. R. Prakash, Universal scaling of the diffusivity of dendrimers in a semidilute solution of linear polymers, *Soft Matter*, 2024, **20**, 993–1008.
52 C. C. Han and A. Z. Akcasu, Concentration dependence of diffusion coefficient at various molecular weights and temperatures, *Polymer*, 1981, **22**, 1165–1168.
53 U. Roessl, S. Leitgeb and B. Nidetzky, Protein freeze concentration and micro-segregation analysed in a temperature-controlled freeze container, *Biotechnol. Rep.*, 2015, **6**, 108–111.
54 J. Wolfe and G. Bryant, Freezing, drying, and/or vitrification of membrane–solute–water systems, *Cryobiology*, 1999, **39**, 103–129.
55 H. Skaer, B. Le, F. Franks, M. H. Asquith and P. Echlin, Polymeric cryoproteetants in the preservation of biological ultrastructure: III. Morphological aspects, *J. Microsc.*, 1977, **110**, 257–270.
56 M. Rubinstein and R. H. Colby, *Polymer Physics*, Oxford University Press, 2003.
57 R. Asthana and S. N. Tewari, The engulfment of foreign particles by a freezing interface, *J. Mater. Sci.*, 1993, **28**, 5414–5425.
58 L. M. Sander and A. V. Tkachenko, Kinetic pinning and biological antifreezes, *Phys. Rev. Lett.*, 2004, **93**, 128102.
59 R. Dou, *et al.*, Hydrogen bonding regulation on phase change in stimuli responsive copolymer aqueous solution, *Polym. Test.*, 2024, **131**, 108324.
60 A. George, H. Varghese, A. Chandran, K. P. Surendran and E. B. Gowd, Directional freezing-induced self-poled piezoelectric nylon 11 aerogels as high-performance mechanical energy harvesters, *J. Mater. Chem. A*, 2024, **12**, 911–922.

61 S. A. Tolba and W. Xia, Molecular insights into the hydration of zwitterionic polymers, *Mol. Syst. Des. Eng.*, 2023, **8**, 1040–1048.
62 T. Inada and S.-S. Lu, Inhibition of recrystallization of ice grains by adsorption of poly (vinyl alcohol) onto ice surfaces, *Cryst. Growth Des.*, 2003, **3**, 747–752.
63 M. Chasnitsky and I. Braslavsky, Ice-binding proteins and the applicability and limitations of the kinetic pinning model, *Philos. Trans. R. Soc., A*, 2019, **377**, 20180391.
64 P. M. Naullage, L. Lupi and V. Molinero, Molecular recognition of ice by fully flexible molecules, *J. Phys. Chem. C*, 2017, **121**, 26949–26957.
65 P. M. Naullage and V. Molinero, Slow propagation of ice binding limits the ice-recrystallization inhibition efficiency of PVA and other flexible polymers, *J. Am. Chem. Soc.*, 2020, **142**, 4356–4366.
66 H. Farag and B. Peters, Engulfment avalanches and thermal hysteresis for antifreeze proteins on supercooled ice, *J. Phys. Chem. B*, 2023, **127**, 5422–5431.
67 H. Farag and B. Peters, Free energy barriers for anti-freeze protein engulfment in ice: Effects of supercooling, footprint size, and spatial separation, *J. Chem. Phys.*, 2023, **158**, 094501.
68 F. Bachtiger, T. R. Congdon, C. Stubbs, M. I. Gibson and G. C. Sosso, The atomistic details of the ice recrystallisation inhibition activity of PVA, *Nat. Commun.*, 2021, **12**, 1323.
69 N. S. Vail, C. Stubbs, C. I. Biggs and M. I. Gibson, Ultralow dispersity poly (vinyl alcohol) reveals significant dispersity effects on ice recrystallization inhibition activity, *ACS Macro Lett.*, 2017, **6**, 1001–1004.
70 A. U. Thosar, *et al.*, On the engulfment of antifreeze proteins by ice, *Proc. Natl. Acad. Sci. U. S. A.*, 2024, **121**, e2320205121.
71 J. Gerhauser and V. Gaukel, Detailed analysis of the ice surface after binding of an insect antifreeze protein and correlation with the Gibbs–Thomson equation, *Langmuir*, 2021, **37**, 11716–11725.
72 M. J. Shultz, E. F. Gubbins, R. G. Davies, Z. Lin and Z. Xiong, Ice interfaces: vapor, liquid, and solutions, *J. Phys. Chem. C*, 2024, **128**, 12326–12338.
73 M. Chasnitsky, S. R. Cohen, Y. Rudich and I. Braslavsky, Atomic force microscopy imaging of ice crystal surfaces formed in aqueous solutions containing ice-binding proteins, *J. Cryst. Growth*, 2023, **601**, 126961.
74 M.-A. Shahbazi, M. Ghalkhani and H. Maleki, Directional freeze-casting: A bioinspired method to assemble multifunctional aligned porous structures for advanced applications, *Adv. Eng. Mater.*, 2020, **22**, 2000033.
75 A. Huerre, C. Josserand and T. Séon, Freezing and capillarity, *Annu. Rev. Fluid Mech.*, 2025, **57**, 257–284.
76 A. W. Rempel and M. G. Worster, Particle trapping at an advancing solidification front with interfacial-curvature effects, *J. Cryst. Growth*, 2001, **223**, 420–432.
77 T. Zhang, Z. Wang, L. Wang, J. Li and J. Wang, Tilting behavior of lamellar ice tip during unidirectional freezing of aqueous solutions, *Langmuir*, 2021, **37**, 10579–10587.
78 M. W. Pot, *et al.*, Versatile wedge-based system for the construction of unidirectional collagen scaffolds by directional freezing: practical and theoretical considerations, *ACS Appl. Mater. Interfaces*, 2015, **7**, 8495–8505.
79 B. M. Guerreiro, L. T. Lou, B. Rubinsky and F. Freitas, Ice modulatory effect of the polysaccharide FucoPol in directional freezing, *Soft Matter*, 2023, **19**, 8978–8987.
80 T. Zhang, L. Wang, Z. Wang, J. Li and J. Wang, Single ice crystal growth with controlled orientation during directional freezing, *J. Phys. Chem. B*, 2021, **125**, 970–979.
81 L. L. C. Olijve, *et al.*, Blocking rapid ice crystal growth through nonbasal plane adsorption of antifreeze proteins, *Proc. Natl. Acad. Sci. U. S. A.*, 2016, **113**, 3740–3745.
82 N. Judge, *et al.*, High molecular weight polyproline as a potential biosourced ice growth inhibitor: synthesis, ice recrystallization inhibition, and specific ice face binding, *Biomacromolecules*, 2023, **24**, 2459–2468.
83 W. Yang, Y. Liao and Z. Sun, Atomistic Insights into the Chain-Length-Dependent Antifreeze Activity of Oligoprolines, *Biomacromolecules*, 2025, 4886–4897.
84 E. F. Gubbins, *et al.*, Phase-sensitive SFG of poly (vinyl alcohol) on calcium fluoride: Interaction with water using backside geometry, *J. Phys. Chem. A*, 2025, 6748–6758.
85 J. Gummel, Y. Roiter, V. Agostiniano, K. Goodall and E. Fratini, Defining the Conformation of Water-Soluble Poly (vinyl alcohol) in Solution: A SAXS, DLS, and AFM Study, *ACS Omega*, 2025, **10**, 18840–18847.
86 L. Almásy, *et al.*, Structure and intermolecular interactions in aqueous solutions of polyethylene glycol, *Molecules*, 2022, **27**, 2573.
87 M. P. Taylor, Confinement free energy for a polymer chain: Corrections to scaling, *J. Chem. Phys.*, 2022, **157**, 094902.
88 A. N. Semenov and A. Johner, Theoretical notes on dense polymers in two dimensions, *Eur. Phys. J. E:Soft Matter Biol. Phys.*, 2003, **12**, 469–480.
89 M. O. Alziyadi and A. R. Denton, Osmotic pressure and swelling behavior of ionic microcapsules, *J. Chem. Phys.*, 2021, **155**, 214904.
90 W. W. Graessley, *Polymeric Liquids & Networks: Structure and Properties*, Garland Science, 2003.
91 Y. Wang, J. Fu, M. Liu, Q. Fu and J. Zhang, Understanding the effect of chain entanglement state on melt crystallization of the polymer freeze-extracted from solution: The role of critical overlap concentration, *Polymer*, 2019, **178**, 121588.
92 L. P. Chang and H. Morawetz, Study of the interpenetration of monodisperse polystyrene in semidilute solution by fluorescence after freeze-drying, *Macromolecules*, 1987, **20**, 428–431.
93 W. Zhang, E. D. Gomez and S. T. Milner, Surface-induced chain alignment of semiflexible polymers, *Macromolecules*, 2016, **49**, 963–971.
94 N. Pertaya, *et al.*, Fluorescence microscopy evidence for quasi-permanent attachment of antifreeze proteins to ice surfaces, *Biophys. J.*, 2007, **92**, 3663–3673.

95 K. Basu, *et al.*, Determining the ice-binding planes of antifreeze proteins by fluorescence-based ice plane affinity, *J. Visualized Exp.*, 2014, 51185.
96 T. Congdon, R. Notman and M. I. Gibson, Antifreeze (glyco) protein mimetic behavior of poly (vinyl alcohol): detailed structure ice recrystallization inhibition activity study, *Biomacromolecules*, 2013, **14**, 1578–1586.
97 J. You, *et al.*, Interactions between nanoparticles and polymers in the diffusion boundary layer during freezing colloidal suspensions, *Langmuir*, 2019, **35**, 10446–10452.
98 H. K. Nguyen, *et al.*, Dynamics gradient of polymer chains near a solid interface, *ACS Macro Lett.*, 2019, **8**, 1006–1011.
99 P. M. Hunger, A. E. Donius and U. G. K. Wegst, Structure–property-processing correlations in freeze-cast composite scaffolds, *Acta Biomater.*, 2013, **9**, 6338–6348.
100 S. S. L. Peppin, M. G. Worster and J. S. Wettlaufer, Morphological instability in freezing colloidal suspensions, *Proc. R. Soc. A*, 2007, **463**, 723–733.
101 Q. Qin and G. B. McKenna, Melting of solvents nanoconfined by polymers and networks, *J. Polym. Sci., Part B: Polym. Phys.*, 2006, **44**, 3475–3486.
102 J. Wu and G. B. McKenna, Anomalous melting behavior of cyclohexane and cyclooctane in poly (dimethyl siloxane) precursors and model networks, *J. Polym. Sci., Part B: Polym. Phys.*, 2008, **46**, 2779–2791.
103 T. Inada and P. R. Modak, Growth control of ice crystals by poly (vinyl alcohol) and antifreeze protein in ice slurries, *Chem. Eng. Sci.*, 2006, **61**, 3149–3158.
104 Y. Yeh and R. E. Feeney, Antifreeze proteins: structures and mechanisms of function, *Chem. Rev.*, 1996, **96**, 601–618.
105 J. S. Vrentas, J. L. Duda and L. W. Ni, Concentration dependence of polymer self-diffusion coefficients, *Macromolecules*, 1983, **16**, 261–266.
106 S. Y. Lee, *et al.*, Janus regulation of ice growth by hyperbranched polyglycerols generating dynamic hydrogen bonding, *Nat. Commun.*, 2022, **13**, 6532.
107 S. Tyagi, C. Monteux and S. Deville, Multiple objects interacting with a solidification front, *Sci. Rep.*, 2021, **11**, 3513.
108 J. G. Meijer, V. Bertin and D. Lohse, Frozen Cheerios effect: Particle-particle interaction induced by an advancing solidification front, *Phys. Rev. Fluids*, 2025, **10**, 34002.
109 T.-H. Fan, *et al.*, Phase-field modeling of freeze concentration of protein solutions, *Polymers*, 2018, **11**, 10.
110 J. A. W. Elliott and S. S. L. Peppin, Particle trapping and banding in rapid colloidal solidification, *Phys. Rev. Lett.*, 2011, **107**, 168301.
111 C. Körber, G. Rau, M. D. Cosman and E. G. Cravalho, Interaction of particles and a moving ice-liquid interface, *J. Cryst. Growth*, 1985, **72**, 649–662.
112 O. Miyawaki, L. Liu and K. Nakamura, Effective partition constant of solute between ice and liquid phases in progressive freeze-concentration, *J. Food Sci.*, 1998, **63**, 756–758.
113 A. Kundagrami and M. Muthukumar, Continuum theory of polymer crystallization, *J. Chem. Phys.*, 2007, **126**, 144901.
114 T. Pinomaa, A. Laukkanen and N. Provatas, Solute trapping in rapid solidification, *MRS Bull.*, 2020, **45**, 910–915.
115 N. Ren, *et al.*, Solute trapping and non-equilibrium microstructure during rapid solidification of additive manufacturing, *Nat. Commun.*, 2023, **14**, 7990.
116 M. J. Aziz and T. Kaplan, Model for solute redistribution during rapid solidification, *Acta Metall.*, 1988, **36**, 2335–2347.
117 H. D. Willauer, J. G. Huddleston and R. D. Rogers, Solute partitioning in aqueous biphasic systems composed of polyethylene glycol and salt: the partitioning behavior of small neutral molecules, *J. Chromatogr. B:Anal. Technol. Biomed. Life Sci.*, 2002, **711**, 201–209.
118 X. Li, M. Wei, H. Yang, Q. Wang and H. Jiang, Dendritic Morphology and Growth Inhibition of Ice Crystals in Sucrose Solutions, *Langmuir*, 2022, **38**, 935–944.
119 S. P. Kharal and J.-F. Louf, Unidirectional freezing of polymer solution droplets, *Langmuir*, 2023, **40**, 118–124.
120 J. P. M. Sousa, *et al.*, Comparative analysis of aligned and random amniotic membrane-derived cryogels for neural tissue repair, *Biomater. Sci.*, 2024, **12**, 4393–4406.
121 W. Lei, *et al.*, Diffusion–Freezing-Induced Microphase Separation for Constructing Large-Area Multiscale Structures on Hydrogel Surfaces, *Adv. Mater.*, 2019, **31**, 1808217.
122 V. Berejnov, N. S. Husseini, O. A. Alsaied and R. E. Thorne, Effects of cryoprotectant concentration and cooling rate on vitrification of aqueous solutions, *Appl. Crystallogr.*, 2006, **39**, 244–251.
123 C. Alba-Simionesco, *et al.*, Interplay of vitrification and ice formation in a cryoprotectant aqueous solution at low temperature, *Proc. Natl. Acad. Sci. U. S. A.*, 2022, **119**, e2112248119.
124 Y. H. Roos, Glass transition and re-crystallization phenomena of frozen materials and their effect on frozen food quality, *Foods*, 2021, **10**, 447.
125 L. Chen, C. Zhao, J. Huang, J. Zhou and M. Liu, Enormous-stiffness-changing polymer networks by glass transition mediated microphase separation, *Nat. Commun.*, 2022, **13**, 6821.
126 L. Peng, *et al.*, Characterization of a novel polyvinyl alcohol/chitosan porous hydrogel combined with bone marrow mesenchymal stem cells and its application in articular cartilage repair, *BMC Musculoskeletal Disord.*, 2019, **20**, 257.
127 J. Song, *et al.*, Freezing-mediated formation of supraproteins using depletion forces, *J. Colloid Interface Sci.*, 2024, **665**, 622–633.
128 P. S. Yu, C. U. Kim and J.-B. Lee, Cryogenic single-molecule fluorescence imaging, *BMB Rep.*, 2025, **58**, 2.
129 Q. Niu and D. Wang, Probing the polymer anomalous dynamics at solid/liquid interfaces at the single-molecule level, *Curr. Opin. Colloid Interface Sci.*, 2019, **39**, 162–172.
130 A. Inagawa, *et al.*, Viscosity of freeze-concentrated solution confined in micro/nanospace surrounded by ice, *J. Phys. Chem. C*, 2017, **121**, 12321–12328.

131 S. Tyagi, C. Monteux and S. Deville, Solute effects on the dynamics and deformation of emulsion droplets during freezing, *Soft Matter*, 2022, **18**, 4178–4188.
132 N. Zhu, Y. Yang, M. Ji, D. Wu and K. Chen, Label-free visualization of lignin deposition in loquats using complementary stimulated and spontaneous Raman microscopy, *Hortic. Res.*, 2019, **6**, 72.
133 E. Pancani, *et al.*, High-resolution label-free detection of biocompatible polymeric nanoparticles in cells, *Part. Part. Syst. Charact.*, 2018, **35**, 1700457.
134 S. Xu, C. H. Camp Jr and Y. J. Lee, Coherent anti-Stokes Raman scattering microscopy for polymers, *J. Polym. Sci.*, 2022, **60**, 1244–1265.
135 N. L. Garrett, *et al.*, Label-free imaging of polymeric nanomedicines using coherent anti-stokes Raman scattering microscopy, *J. Raman Spectrosc.*, 2012, **43**, 681–688.
136 C. Ceconello, *et al.*, *Wide-field broadband CARS microscopy*, in *EPJ Web of Conferences*, 2022, vol. 266, p. 8001.
137 D. Gudavičius, L. Kontenis and W. Langbein, Thousand foci coherent anti-Stokes Raman scattering microscopy, *APL Photonics*, 2024, **9**, 086110.
138 M. Mittal, J. A. Roper III, C. L. Jackson, G. G. Monaghan and L. F. Francis, Effects of freezing and thawing on the microstructure of latex paints, *J. Colloid Interface Sci.*, 2013, **392**, 183–193.
139 J. Liang, X. Xiao, T.-M. Chou and M. Libera, Counterion exchange in peptide-complexed core–shell microgels, *Langmuir*, 2019, **35**, 9521–9528.
140 M. Kurozumi, Y. Yano, S. Kiyoyama, A. Kumar and K. Shiomori, Adsorption properties of arsenic(V) by polyacrylamide cryogel containing iron hydroxide oxide particles prepared by in situ method, *Resour. Proc.*, 2015, **62**, 17–23.
141 E. S. Dragan, M. V. Dinu, C. A. Ghiorghita, M. M. Lazar and F. Doroftei, Preparation and characterization of semi-IPN cryogels based on polyacrylamide and poly (N, N-dimethylaminoethyl methacrylate); Functionalization of carrier with monochlorotriazinyl-β-cyclodextrin and release kinetics of curcumin, *Molecules*, 2021, **26**, 6975.
142 A. Cecilia, *et al.*, Optimizing structural and mechanical properties of cryogel scaffolds for use in prostate cancer cell culturing, *Mater. Sci. Eng., C*, 2017, **71**, 465–472.
143 W. Li, *et al.*, Synchrotron Radiation X-ray Scattering Approaching Real Industrial Processing of Polymer, *Polym. Sci. Technol.*, 2025, **1**, 155–170.
144 R. Ortega, *et al.*, Native cryo-correlative light and synchrotron X-ray fluorescence imaging of proteins and essential metals in subcellular neuronal compartments, *Chem. Biomed. Imaging*, 2024, **2**, 744–754.
145 P. H. Kamm, *et al.*, X-Ray Tomoscopy Reveals the Dynamics of Ice Templating, *Adv. Funct. Mater.*, 2023, **33**, 2304738.
146 J. D. Moon, *et al.*, Nanoscale water–polymer interactions tune macroscopic diffusivity of water in aqueous poly (ethylene oxide) solutions, *Chem. Sci.*, 2024, **15**, 2495–2508.
147 C. Poelma, Measurement in opaque flows: a review of measurement techniques for dispersed multiphase flows, *Acta Mech.*, 2020, **231**, 2089–2111.
148 V. Ayel, O. Lottin, M. Faucheux, D. Sallier and H. Peerhossaini, Crystallisation of undercooled aqueous solutions: Experimental study of free dendritic growth in cylindrical geometry, *Int. J. Heat Mass Transfer*, 2006, **49**, 1876–1884.
149 H. Schoof, L. Bruns, A. Fischer, I. Heschel and G. Rau, Dendritic ice morphology in unidirectionally solidified collagen suspensions, *J. Cryst. Growth*, 2000, **209**, 122–129.
150 W. W. Mullins and R. F. Sekerka, Stability of a planar interface during solidification of a dilute binary alloy, *J. Appl. Phys.*, 1964, **35**, 444–451.
151 J.-W. Kim, K. Taki, S. Nagamine and M. Ohshima, Preparation of porous poly (L-lactic acid) honeycomb monolith structure by phase separation and unidirectional freezing, *Langmuir*, 2009, **25**, 5304–5312.
152 X. Song, M. A. Philpott, S. M. Best and R. E. Cameron, Controlling the architecture of freeze-dried collagen scaffolds with ultrasound-induced nucleation, *Polymers*, 2024, **16**, 213.
153 P. Divakar, K. Yin and U. G. K. Wegst, Anisotropic freeze-cast collagen scaffolds for tissue regeneration: How processing conditions affect structure and properties in the dry and fully hydrated states, *J. Mech. Behav. Biomed. Mater.*, 2019, **90**, 350–364.
154 C. Su, H. Wang, W. Cai and X. Shao, Ice growth inhibition by poly (vinyl alcohol): Insights from near-infrared spectroscopy and molecular dynamics simulation, *J. Mol. Liq.*, 2024, **402**, 124795.
155 S. S. L. Peppin, J. A. W. Elliott and M. G. Worster, Solidification of colloidal suspensions, *J. Fluid Mech.*, 2006, **554**, 147–166.
156 E. Buratti, *et al.*, The role of polymer structure on water confinement in poly (N-isopropylacrylamide) dispersions, *J. Mol. Liq.*, 2022, **355**, 118924.
157 P. Linse and N. Kallrot, Polymer adsorption from bulk solution onto planar surfaces: effect of polymer flexibility and surface attraction in good solvent, *Macromolecules*, 2010, **43**, 2054–2068.
158 N. Joshi, K. Suman and Y. M. Joshi, Rheological behavior of aqueous poly (vinyl alcohol) solution during a freeze–thaw gelation process, *Macromolecules*, 2020, **53**, 3452–3463.
159 J. Dhainaut, G. Piana, S. Deville, C. Guizard and M. Klotz, Freezing-induced ordering of block copolymer micelles, *Chem. Commun.*, 2014, **50**, 12572–12574.
160 A. Suzuki and H. Yui, Crystallization of confined water pools with radii greater than 1 nm in AOT reverse micelles, *Langmuir*, 2014, **30**, 7274–7282.
161 D. A. Fedosov, G. E. Karniadakis and B. Caswell, Dissipative particle dynamics simulation of depletion layer and polymer migration in micro-and nanochannels for dilute polymer solutions, *J. Chem. Phys.*, 2008, **128**, 144903.

162 E. V. Makoveeva, I. E. Koroznikova, A. E. Glebova and D. V. Alexandrov, Morphological/dynamic instability of directional crystallization in a finite domain with intense convection, *Crystals*, 2023, **13**, 1276.
163 F. Leoni, E. C. Oğuz and G. Franzese, Emergence of disordered hyperuniformity in confined fluids and soft matter, *arXiv*, 2024, preprint, arXiv:2411.12393, DOI: 10.48550/arXiv.2411.12393.
164 J. Jiang, G. X. Li, Q. Sheng and G. H. Tang, Microscopic mechanism of ice nucleation: The effects of surface rough structure and wettability, *Appl. Surf. Sci.*, 2020, **510**, 145520.
165 S. Keshavarzi, A. Entezari, K. Maghsoudi, G. Momen and R. Jafari, Ice nucleation on silicone rubber surfaces differing in roughness parameters and wettability: Experimental investigation and machine learning–based predictions, *Cold Reg. Sci. Technol.*, 2022, **203**, 103659.
166 F. Wang, *et al.*, The three-line synergistic icephobicity of conductive CNTs/PDMS nanocomposite with bio-inspired hierarchical surface, *Surf. Interfaces*, 2021, **26**, 101424.
167 M. Kaneda, Y. Takao and J. Fukai, Thermal and solutal effects on convection inside a polymer solution droplet on a substrate, *Int. J. Heat Mass Transfer*, 2010, **53**, 4448–4457.
168 S. Hasan, *et al.*, Direct characterization of solute transport in unsaturated porous media using fast X-ray synchrotron microtomography, *Proc. Natl. Acad. Sci. U. S. A.*, 2020, **117**, 23443–23449.
169 C. J. Werth, C. Zhang, M. L. Brusseau, M. Oostrom and T. Baumann, A review of non-invasive imaging methods and applications in contaminant hydrogeology research, *J. Contam. Hydrol.*, 2010, **113**, 1–24.
170 I. Aranaz, M. C. Gutiérrez, M. L. Ferrer and F. Del Monte, Preparation, of chitosan nanocompositeswith a macroporous structure by unidirectional freezing and subsequent freeze-drying, *Mar. Drugs*, 2014, **12**, 5619–5642.
171 A. M. Anderson and M. G. Worster, Periodic ice banding in freezing colloidal dispersions, *Langmuir*, 2012, **28**, 16512–16523.
172 S. Deville, J. Adrien, E. Maire, M. Scheel and M. Di Michiel, Time-lapse, three-dimensional in situ imaging of ice crystal growth in a colloidal silica suspension, *Acta Mater.*, 2013, **61**, 2077–2086.
173 M. Razavi, Y. Qiao and A. S. Thakor, Three-dimensional cryogels for biomedical applications, *J. Biomed. Mater. Res., Part A*, 2019, **107**, 2736–2755.
174 S. V. German, G. S. Budylin, E. A. Shirshin and D. A. Gorin, Advanced technique for in situ Raman spectroscopy monitoring of the freezing-induced loading process, *Langmuir*, 2021, **37**, 1365–1371.
175 A. Twomey, R. Less, K. Kurata, H. Takamatsu and A. Aksan, In situ spectroscopic quantification of protein–ice interactions, *J. Phys. Chem. B*, 2013, **117**, 7889–7897.
176 D. Katrantzi, S. Micklethwaite, N. Hondow, A. Brown and L. Dougan, Unveiling the structure of protein-based hydrogels by overcoming cryo-SEM sample preparation challenges, *Faraday Discuss.*, 2025, 55–81.
177 L. Weng, S. L. Stott and M. Toner, Molecular dynamics at the interface between ice and poly (vinyl alcohol) and ice recrystallization inhibition, *Langmuir*, 2017, **34**, 5116–5123.
178 S. Jin, *et al.*, Spreading fully at the ice-water interface is required for high ice recrystallization inhibition activity, *Sci. China:Chem.*, 2019, **62**, 909–915.
179 P. Pal, R. Aich, S. Chakraborty and B. Jana, Molecular factors of ice growth inhibition for hyperactive and globular antifreeze proteins: Insights from molecular dynamics simulation, *Langmuir*, 2022, **38**, 15132–15144.
180 C. I. Biggs, *et al.*, Mimicking the ice recrystallization activity of biological antifreezes. When is a new polymer "active"?, *Macromol. Biosci.*, 2019, **19**, 1900082.
181 C. Budke and T. Koop, Ice recrystallization inhibition and molecular recognition of ice faces by poly (vinyl alcohol), *ChemPhysChem*, 2006, **7**, 2601–2606.
182 X. Yang, *et al.*, Study on the adsorption process of a semiflexible polymer onto homogeneous attractive surfaces, *Polymer*, 2019, **172**, 83–90.
183 Y. Shibuta, Molecular dynamics of solidification, *ISIJ Int.*, 2024, **64**, 1107–1124.
184 G. G. Poon and B. Peters, A stochastic model for nucleation in the boundary layer during solvent freeze-concentration, *Cryst. Growth Des.*, 2013, **13**, 4642–4647.
185 C. Hübner, M. Vadalà, K. Voges and D. C. Lupascu, Poly (vinyl alcohol) freeze casts with nano-additives as potential thermal insulators, *Sci. Rep.*, 2023, **13**, 1020.
186 L. Zhou, S. Zhai, Y. Chen and Z. Xu, Anisotropic cellulose nanofibers/polyvinyl alcohol/graphene aerogels fabricated by directional freeze-drying as effective oil adsorbents, *Polymers*, 2019, **11**, 712.
187 G. Zhao, *et al.*, Anisotropic 3D aerogel of graphene oxide and poly (vinyl alcohol) for desalination by interfacial solar vapor generation, *ACS Appl. Nano Mater.*, 2024, **7**, 18870–18880.
188 J.-H. Lee, *et al.*, Membranes with through-thickness porosity prepared by unidirectional freezing, *Polymer*, 2010, **51**, 6215–6221.
189 Z. Wang, *et al.*, Mechanisms of ice crystal growth in nanoconfined spaces of cementitious composites at low temperatures: Insights from molecular dynamics simulations, *J. Am. Ceram. Soc.*, 2024, **107**, 8396–8414.
190 N. Di Pasquale, *et al.*, Solid–liquid interfacial free energy from computer simulations: challenges and recent advances, *Chem. Rev.*, 2025, **125**, 5003–5053.
191 Y. Qiu, *et al.*, Ice nucleation efficiency of hydroxylated organic surfaces is controlled by their structural fluctuations and mismatch to ice, *J. Am. Chem. Soc.*, 2017, **139**, 3052–3064.
192 K. Mochizuki, Y. Qiu and V. Molinero, Promotion of homogeneous ice nucleation by soluble molecules, *J. Am. Chem. Soc.*, 2017, **139**, 17003–17006.
193 Y. Liu, D. Zhang, Y. Tang, X. Gong and J. Zheng, Development of a radical polymerization algorithm for molecular dynamics simulations of antifreezing hydrogels with double-network structures, *npj Comput. Mater.*, 2023, **9**, 209.

194 A. Milchev and K. Binder, Semiflexible polymers interacting with planar surfaces: Weak versus strong adsorption, *Polymers*, 2020, **12**, 255.
195 G. J. Fleer, Polymers at interfaces and in colloidal dispersions, *Adv. Colloid Interface Sci.*, 2010, **159**, 99–116.
196 G. Shao, D. A. H. Hanaor, X. Shen and A. Gurlo, Freeze casting: from low-dimensional building blocks to aligned porous structures—a review of novel materials, methods, and applications, *Adv. Mater.*, 2020, **32**, 1907176.
197 N. Arai and K. T. Faber, Gradient-controlled freeze casting of preceramic polymers, *J. Eur. Ceram. Soc.*, 2023, **43**, 1904–1911.
198 B. M. Guerreiro, *et al.*, Elevated fucose content enhances the cryoprotective performance of anionic polysaccharides, *Int. J. Biol. Macromol.*, 2024, **261**, 129577.
199 F. Ginot, T. Lenavetier, D. Dedovets and S. Deville, Solute strongly impacts freezing under confinement, *Appl. Phys. Lett.*, 2020, **116**, 253701.
200 L. Sun, Z. Zhu and D.-W. Sun, Regulating ice formation for enhancing frozen food quality: Materials, mechanisms and challenges, *Trends Food Sci. Technol.*, 2023, **139**, 104116.
201 P. G. Georgiou, *et al.*, Polymer self-assembly induced enhancement of ice recrystallization inhibition, *J. Am. Chem. Soc.*, 2021, **143**, 7449–7461.
202 Y. Li, B. C. Abberton, M. Kröger and W. K. Liu, Challenges in multiscale modeling of polymer dynamics, *Polymers*, 2013, **5**, 751–832.
203 R. Mondal and G. Kumaraswamy, Materials prepared by freezing-induced self-assembly of dispersed solutes: a review, *Mater. Adv.*, 2022, **3**, 3041–3054.